Modeling of Ferric Sulfate Decomposition and Sulfation of Potassium Chloride During Grate-Firing of Biomass

Hao Wu, Jacob Boll Jespersen, Flemming Jappe Frandsen, and Peter Glarborg
Dept. of Chemical and Biochemical Engineering, Technical University of Denmark, Søltofts Plads, Building 229, DK-2800 Kgs. Lyngby, Denmark

Martti Aho, Kari Paakkinen, and Raili Taipale
Bioenergy Knowledge Centre, VTT Technical Research Centre of Finland, FI-40101 Jyväskylä, Finland

DOI 10.1002/aic.14174
Published online July 12, 2013 in Wiley Online Library (wileyonlinelibrary.com)

Ferric sulfate is used as an additive in biomass combustion to convert the released potassium chloride to the less harmful potassium sulfate. The decomposition of ferric sulfate is studied in a fast heating rate thermogravimetric analyzer and a volumetric reaction model is proposed to describe the process. The yields of sulfur oxides from ferric sulfate decomposition under boiler conditions are investigated experimentally, revealing a distribution of approximately 40% SO_3 and 60% SO_2. The ferric sulfate decomposition model is combined with a detailed kinetic model of gas-phase KCl sulfation and a model of K_2SO_4 condensation to simulate the sulfation of KCl by ferric sulfate addition. The simulation results show good agreements with experiments conducted in a biomass grate-firing reactor. The results indicate that the SO_3 released from ferric sulfate decomposition is the main contributor to KCl sulfation and that the effectiveness of ferric sulfate addition is sensitive to the applied temperature conditions. © 2013 American Institute of Chemical Engineers *AIChE J*, 59: 4314–4324, 2013

Keywords: biomass combustion, additive, sulfate decomposition, sulfation of potassium chloride, chemical kinetics modeling

Introduction

As an important source of renewable energy, biomass is utilized in heat and/or power generation through different combustion technologies such as grate combustion,[1–6] fluidized bed combustion,[7–9] and pulverized fuel combustion.[10–12] One of the major technical challenges associated with the use of biomass in these applications is that the combustion of biomass may result in a considerable amount of alkali chlorides in the flue gas and subsequently lead to severe ash-deposition and corrosion problems in the boilers.[6,7,10,11,13–17] In order to mitigate the alkali chloride-induced problems in biomass combustion, a feasible method is to use additives to convert the alkali chlorides to less harmful alkali species (such as sulfates or aluminosilicates) and release the chlorine as HCl.[5,9,18–27] In biomass combustion, it is desirable to convert the fuel-chlorine to HCl, as it is not condensable on heat transfer surface and the partial pressure of HCl in biomass-derived flue gas is not high enough to cause severe gas-phase corrosion.[17] On the other hand, the alkali chlorides present in the flue gas can condense on heat transfer surface and induce significant solid/liquid/gas-phase corrosion.[17,28]

Sulfur-based additives, such as elemental sulfur,[9,21,31] SO_2,[29,30] ammonium sulfate,[5,9,22,32–34] aluminum sulfate,[19] and ferric sulfate,[19,31] have been tested in biomass combustion. Thermal decomposition or oxidation of these additives produces SO_2 and SO_3. The latter rapidly converts corrosive alkali chlorides to alkali sulfates and hydrogen chloride under furnace conditions through the following global reaction

$$2MCl + SO_3 + H_2O \rightarrow M_2SO_4 + 2HCl \quad (1)$$

where M is K or Na.

The effectiveness of different sulfur-based additives has been investigated experimentally.[9,19,21,30] Sulfates (such as ammonium sulfate, aluminum sulfate, and ferric sulfate) are in general much more effective than elemental sulfur.[9,19,21] In a biomass-fired boiler where the gas residence time is typically very short (a few seconds), SO_3 is needed in order to achieve a fast sulfation of alkali chlorides. However, the homogeneous oxidation of SO_2 to SO_3 is usually rather limited in the boiler because the reaction is thermodynamically restricted at high temperatures (e.g., above 1100°C) and kinetically limited at low temperatures (e.g., below 900°C).[35,36] Therefore, with the addition of elemental sulfur, only a small fraction would be oxidized to SO_3 and contribute to the formation of alkali sulfates.[21] On the other hand, the thermal decomposition of sulfate additives is believed to produce SO_3

Correspondence concerning this article should be addressed to H. Wu at haw@kt.dtu.dk.

© 2013 American Institute of Chemical Engineers

directly, resulting in a fast sulfation of alkali chlorides.[19,21] Thus, for the same sulfur dosage, a significantly higher sulfation degree on alkali chlorides can be obtained with a sulfate additive as compared to elemental sulfur or SO_2.[21,31]

In spite of the extensive experimental studies on the utilization of sulfate additives,[5,9,19,21–23,34] investigations on the decomposition rate and products (e.g., the distribution between the produced SO_2 and SO_3) of these additives are scarce. In relation to this, no modeling work has been carried out to simultaneously simulate the decomposition of the sulfate additives and the sulfation of potassium chloride under biomass-fired boiler conditions. The development of such a model would facilitate the optimization of sulfate additive utilization during biomass combustion.

The objective of this study was to develop a model for the sulfation of potassium chloride by ferric sulfate addition during biomass combustion. The decomposition of ferric sulfate was investigated in a fast heating rate thermogravimetric analyzer (TGA) and a laboratory-scale tube reactor in order to understand the decomposition kinetics and the product distribution. The model developed in this work combined a volumetric reaction model for ferric sulfate decomposition with a detailed gas-phase kinetic model for sulfation of potassium chloride,[35] and a simplified model for homogeneous and heterogeneous condensation of potassium sulfate.[37] It was validated by comparison with experimental results from biomass combustion in a pilot-scale grate reactor, where ferric sulfate was injected in different amounts to the post-flame zone.[31]

Experimental

High heating-rate TGA

Decomposition of ferric sulfate was studied in a Netzsch STA 449 F1 Jupiter TGA under a slow heating rate of 10°C/min and a fast heating rate of 500°C/min, respectively. The experiments were all carried out in a nitrogen environment, with an N_2 flow rate of 25 ml/min. The decomposition rate of ferric sulfate is believed to be independent of the surrounding gas composition, thus the kinetic parameters derived from N_2 environment are applicable to a boiler environment with flue gas containing N_2, O_2, CO_2, H_2O, etc. The sample used in the experiments was a ferric sulfate hydrate ($Fe_2(SO_4)_3{\cdot}xH_2O$) from Sigma-Aldrich with a purity of 97% and an average particle size of 82 μm analyzed by Malvern Mastersizer 2000 particle size analyzer. An alumina crucible with an inner diameter of 15 mm and a depth of 20 mm was used, and the sample mass placed in the crucible was below 10 mg. For the slow heating rate experiments, the ferric sulfate hydrate was heated from 25 to 800°C at 10°C/min. In the fast heating rate experiments, the ferric sulfate hydrate was first dehydrated by heating up to 250°C at 10°C/min. After 30 min holding time, the sample was heated at a rate of 500°C/min to an end temperature, which was varied from 600 to 800°C in intervals of 50°C. Depending on the time needed for complete conversion, the holding time at different end temperatures varied from 90 to 30 min.

Laboratory-scale tube reactor

Experiments in a laboratory-scale tube reactor were conducted to identify the yield of SO_2 and SO_3 from the decomposition of ferric sulfate. The principle of the setup has been described in detail in our earlier work.[14,38,39] A brief introduction is provided here. The setup consists of a horizontal ceramic tube reactor with an inner diameter of 50 mm and a length of 1200 mm. During the experiments, the reactor was electrically heated to a desired temperature under a controlled flow of 5 Nl/min N_2. Then a thin layer of ferric sulfate was placed in an alumina boat (sample mass below 1 g) and the boat was inserted into the middle of the reactor. The flue gas from the reactor was analyzed for SO_2 and O_2 by two Fischer-Rosemount NGA 2000 analyzers using IR method and an electrochemical method based on the current generated by oxygen reduction over a gold electrode, respectively. The accuracy of the analyzers was ±2.7%, including the uncertainties of both the instrument and the calibration gases. The experiment was terminated when the SO_2 concentration in the flue gas had decreased to below 1 ppm, indicating that complete conversion of the ferric sulfate was achieved. Following the approach of Nielsen et al.,[39] the amount of SO_2 released from the decomposition of ferric sulfate was quantified by integrating the measured SO_2 concentration over time. Based on the amount of the input ferric sulfate, a fractional conversion of the sulfur in ferric sulfate to SO_2 was calculated. The remaining sulfur in ferric sulfate is assumed to be released as SO_3. According to global equilibrium calculations (in FactSage 6.2, database Fact53), ferric sulfate decomposition is unlikely to yield sulfur species other than SO_2 and SO_3 in an inert environment.

The ferric sulfate used in the tube reactor experiments was produced from the hydrate used in the TGA experiments. In order to achieve a complete dehydration, the ferric sulfate hydrate was heated to 400°C for 1 h and then cooled down to room temperature in an inert environment (N_2). The produced ferric sulfate was kept in a desiccator in order to avoid reactions with moisture in air.

The decomposition of ferric sulfate was studied in the tube reactor at temperatures varying from 600 to 1000°C; a temperature range, where homogeneous decomposition of SO_3 to SO_2 is expected to be insignificant. In addition, this temperature range is representative of the conditions in the grate boiler where ferric sulfate was used as an additive.[31] In order to ensure the reliability of the results, a number of repetition experiments (3–5 times) were performed under the same operating conditions.

Pilot-scale grate-firing reactor

In order to investigate the effect of ferric sulfate addition on the destruction of potassium chloride during grate-firing of biomass, a series of experiments has been carried out in a 100 kW grate reactor located at the VTT Technical Research Centre of Finland.[31] The data from the experimental campaign are used for model validation in this work. The details regarding the experimental setup, procedures, and results have been described elsewhere.[31] A brief introduction is provided here.

A schematic diagram of the combustor and the locations of the sampling ports are shown in Figure 1. The inner furnace diameter of the reactor is 400 mm. During the experiments, the combustion of the biomass took place on a rotating grate, equipped with narrow primary air inlets. Secondary air was injected above the grate to facilitate complete combustion, with the ratio between primary and secondary air maintained as 1:1.

The fuel used in the experiments was a mixture of Spanish wood chips and 40 ± 4% (energy basis) corn stover, with

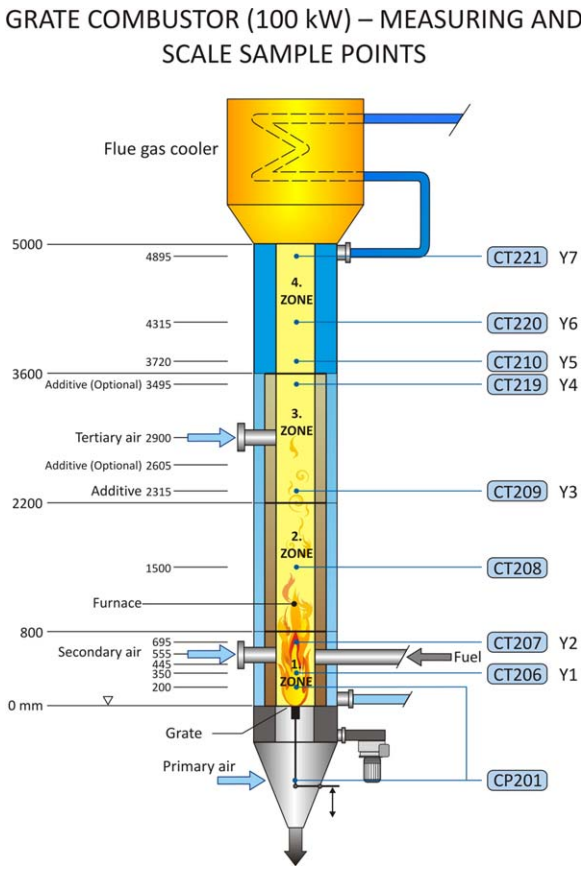

Figure 1. A schematic diagram of the 100 kW grate combustor at VTT Technical Research Centre of Finland.[40]

[Color figure can be viewed in the online issue, which is available at wileyonlinelibrary.com].

analyzed compositions as shown in Table 1. A constant fuel load of 89 ± 5 kW secured temperature versus residence time profiles in the freeboard that were representative of a grate-fired power plant, operated at full load with the same biomass mixture.[31] The excess air ratio during the experiments was controlled to be around 1.46. The temperatures in the freeboard above the grate were measured by a suction pyrometer at different sampling ports. At port Y5, an impactor was used to sample the alkali vapors and small particulates generated from combustion. The impactor was operated at room temperature, and the flue gas sending to the impactor was diluted by nitrogen with a dilution ratio varying in a range of 12–21. Therefore, it is believed that all of the ash forming species in the fuel gas would be collected as aerosols in the impactor. The chemical composition of the collected aerosols was analyzed by flame atomic absorption spectrometry (FAAS) and ion chromatography (IC).[40] The flue gas was analyzed by traditional online analyzers for O_2, CO, CO_2, and NO after the cyclone, placed downstream of the flue gas cooler. In addition, a flue gas flow was sampled at port Y7 to measure HCl and SO_2 through a FTIR analyzer.[40] For the experiments with ferric sulfate addition, an aqueous solution of ferric sulfate (up to 25 wt %) was sprayed into the furnace via port Y3 (see Figure 1) with a constant flow rate of 15 ml/min and an average droplet size of about 12 μm. The dosage of ferric sulfate, determined as the molar ratio of $S_{reagent}/Cl_{fuel}$, was varied through changing the concentration of the ferric sulfate solution. The results shown in this work were based on $S_{reagent}/Cl_{fuel}$ ratios of 0, 0.4, 0.6, 0.8, and 1.0, respectively.

Table 1. Fuel Analysis of a Mixture of 60% Wood Chips and 40% Corn Stover (energy basis)[31]

Analysis (unit)	Value
Moisture (wt %)	29
LHV (as received) (MJ/kg)	10.7
Ash (wt % dry)	8.0
S (wt % dry)	0.04
Cl (wt % dry)	0.24
C (wt % dry)	45.42[a]
H (wt % dry)	5.69[a]
N (wt % dry)	0.32[a]
F (wt % dry)	0.01[a]
Br (wt % dry)	<0.001[a]
K (wt % dry)	0.83[b]
Na (wt % dry)	0.07[b]

[a]Based on the analysis of pure wood and corn stover.[40]
[b]Based on the K and Na content of pure wood and corn stove.[41]

Model Development and Simulation

The model developed in this work involves a description of ferric sulfate decomposition, a detailed reaction mechanism for the gas-phase reactions of SO_2/SO_3 and KCl,[35] and a simplified model for homogeneous condensation of K_2SO_4.[37] These submodels are introduced in the following along with the input parameters and the simulation procedures.

Decomposition of ferric sulfate

Figure 2 shows the decomposition behavior of ferric sulfate hydrate during the TGA experiment at a slow heating rate (10°C/min). Two major mass-loss steps are observed. The first step, which we attribute to dehydration, occurs in a temperature range of 150–200°C. The second step, at temperatures of 550–700°C, is attributed to the decomposition of anhydrous ferric sulfate ($Fe_2(SO_4)_3$) to Fe_2O_3, based on the observed mass loss caused by the formation of SO_3 and/or $SO_2 + O_2$. The temperature range for the decomposition is in agreement with values reported elsewhere for anhydrous ferric sulfate.[42–45]

For deriving the kinetic parameters of ferric sulfate decomposition, the relative mass (W) of the anhydrous ferric sulfation is defined as

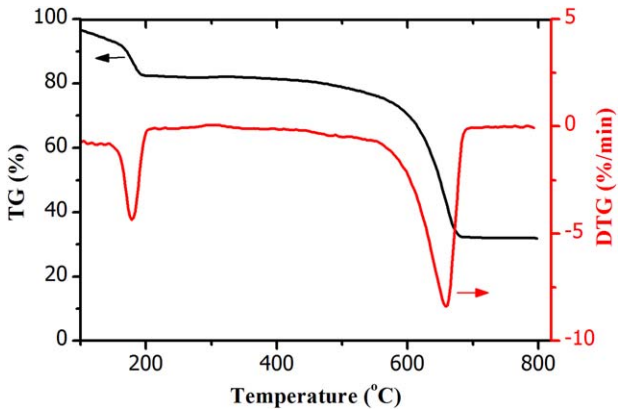

Figure 2. TG and DTG curves of ferric sulfate hydrate decomposition under nitrogen environment with a heating rate of 10°C/min.

[Color figure can be viewed in the online issue, which is available at wileyonlinelibrary.com].

$$W = \frac{m - m_\infty}{m_0 - m_\infty} \quad (2)$$

where m_0 (g) is the mass of the anhydrous ferric sulfate before decomposition, m_∞ (g) is the mass of the residue after decomposition, and m (g) is the mass of anhydrous ferric sulfate at t(s) during decomposition.

In present study, the decomposition of ferric sulfate in the TGA is assumed to follow the volumetric reaction model described by the equation

$$\frac{dW}{dt} = -kW \quad (3)$$

The assumption of a volumetric reaction model is supported by SEM-EDS (scanning electron microscopy and dispersive X-ray spectroscopy) analysis of the partially converted ferric sulfate particles (see Figure 3). The molar ratio of Fe/S is rather consistent over the sectioned particle, suggesting that the decomposition reaction takes place in the entire particle. Therefore, we believe that the volumetric reaction model is more suitable than the shrinking core model used in literature[42] to describe the decomposition reaction.

The rate constant k in Eq. 3 is assumed to follow an Arrhenius expression

$$k = A \cdot \exp\left(-\frac{E}{RT}\right) \quad (4)$$

where $A(s^{-1})$ is the pre-exponential factor, E(kJ/mol) is the activation energy, R(kJ/mol/K) is the gas constant, and T(K) is the temperature of the particle. The activation energy (E) and the pre-exponential factor (A) in Eq. 4 can be derived from the TGA data. For the TGA experiments with a constant slow heating rate of 10°C/min, the following correlation is used to derive the kinetic parameters, by plotting the left side of the equation against $1/T$

$$\ln\left(-\frac{\left(\frac{dW}{dt}\right)}{W}\right) = \ln(A) - \frac{E}{RT} \quad (5)$$

In this work, the kinetic parameters derived from Eq. 5 are based on a conversion of 10–90%, as the noise level of the data is more significant when the conversion is below 10% or above 90%.

For the TGA experiments with a high heating rate (500°C/min), an isothermal condition is achieved when the predefined end temperature is reached. The data recorded from the isothermal period are chosen to derive kinetic parameters. Under isothermal conditions, Eq. 3 can be integrated and rewritten as

$$\ln(W) = -kt + \ln(W_0) \quad (6)$$

where t(s) is the residence time under isothermal condition, and W_0 is the relative mass of the anhydrous ferric sulfate when the isothermal condition is reached. Based on Eq. 6, the rate constant k at a specific temperature is obtained by plotting the left side of the equation against t(s). With a value of k derived at different temperatures (T), the activation energy (E) and the pre-exponential factor (A) can be obtained by plotting $\ln(k)$ against $1/T$. The isothermal kinetic parameters are also obtained based on a conversion up to 90%, in order to minimize the uncertainty caused by the small mass of residual sample.

Figure 4 compares the rate constants derived from the isothermal and nonisothermal TGA experiments in this study with data from literature.[42] The kinetic parameters are listed in Table 2. For the isothermal experiments, a high linearity is seen between $\ln(k)$ and $1/T$, indicating that the Arrhenius expression of Eq. 4 can satisfactorily describe the decomposition of ferric sulfate under isothermal conditions. The pre-exponential factor and activation energy derived from the nonisothermal experiment are considerably lower than those of the isothermal experiments (Table 2). We attribute this difference to the fact that the isothermal kinetics is derived at higher temperatures than those of the nonisothermal kinetics. For the isothermal kinetics derived from Kolta and Askar,[42] where the applied temperature range is similar to the nonisothermal experiment in this study, the kinetic parameters are in close agreement (Figure 4). The results of Figure 4 imply that the kinetic parameters derived from low temperatures (e.g., those from the nonisothermal experiments of this work or isothermal experiments of Kolta and Askar[42]) may not be directly extrapolated to higher temperatures (e.g., the temperature range of the isothermal experiments of this work). For the simulation of ferric sulfate decomposition in a grate-firing reactor with high temperatures, we prefer to

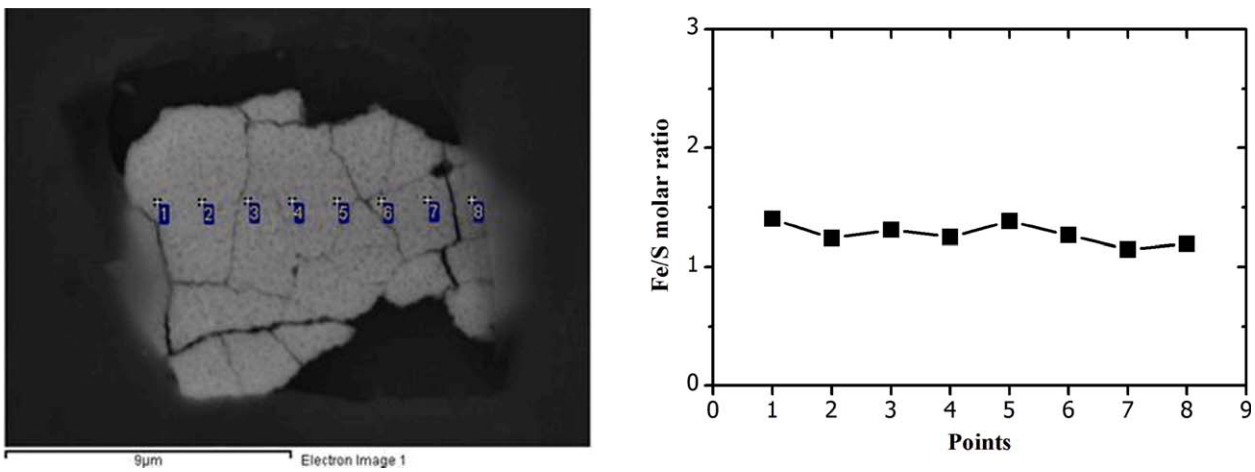

Figure 3. SEM-EDS analysis of the sectioned partially converted ferric sulfate particle.

The left figure shows the SEM image and the right figure shows the Fe/S molar ratio of analyzed spots.

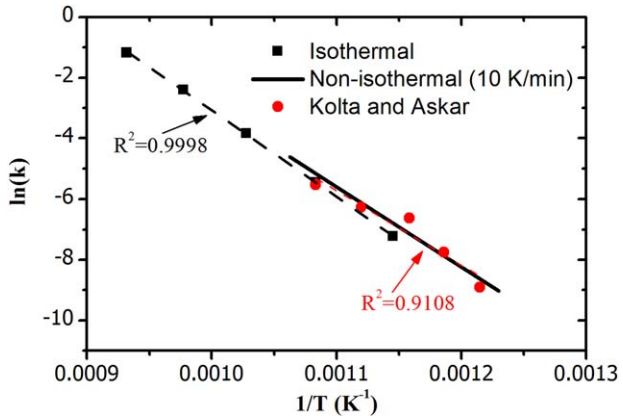

Figure 4. Correlation between ln(k) and 1/T during ferric sulfate decomposition in the TGA experiments of this study and in literature.

For the nonisothermal TGA data, only the temperature range at which the kinetic parameters are derived is plotted. The data of Kolta and Askar is derived from Figure 3 of their paper.[42] [Color figure can be viewed in the online issue, which is available at wileyonlinelibrary.com].

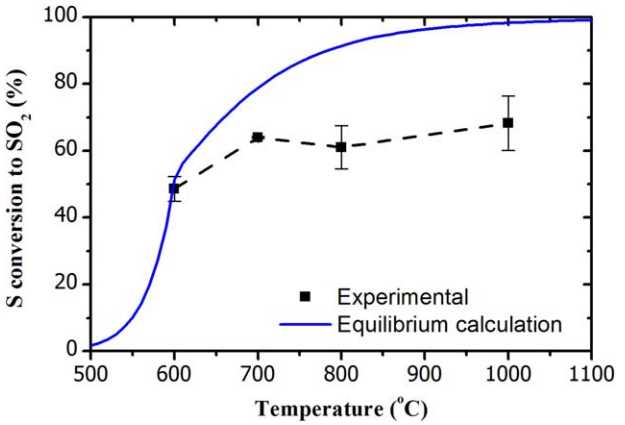

Figure 5. The percentage of sulfur in ferric sulfate converted to SO_2 (%) at different temperatures in a nitrogen environment.

The solid symbols denote the experimental results in the tube reactor, and the solid line denotes the results from global equilibrium calculations in FactSage 6.2 (database: Fact53). The error bars represent the standard deviations of the repeated experiments under the same condition. [Color figure can be viewed in the online issue, which is available at wileyonlinelibrary.com].

use the kinetic parameters obtained from the isothermal TGA experiments, as these parameters are derived from a temperature range closer to the practical conditions.

The results from the laboratory-scale tube reactor experiments are shown in Figure 5, along with results of global equilibrium calculations in FactSage 6.2 using the Fact53 database. At temperatures around 600°C, the conversion of ferric sulfate to SO_2 is about 50%. However, in the temperature range of 700–1000°C, approximately 60% of the sulfur in ferric sulfate is released as SO_2. This value is generally below that predicted from global equilibrium (see Figure 5), indicating that the conversion from SO_3 to SO_2 is kinetically limited in this temperature range. This observation is in agreement with the experimental study of Yilmaz et al.,[46] where thermal dissociation of SO_3 was found be slow below 1000°C. On the other hand, at low temperatures such as 600°C, the distribution of SO_2 and SO_3 appears to be closer to the equilibrium curve in Figure 5. It is likely that ferric oxide (formed during the ferric sulfate decomposition) catalyzes interconversion between SO_2 and SO_3.[36] As the temperature increases, the decomposition of ferric sulfate becomes faster and the contact time between SO_x and the solid particle (catalyst) reduces. As the decomposition of ferric sulfate upon injection in a furnace primarily occurs at temperatures above 700°C, it is reasonable to assume for modeling purposes that the decomposition of ferric sulfate under boiler conditions constantly releases 60% of the sulfur as SO_2 and 40% of the sulfur as SO_3. Based on this assumption, we propose the following global reaction for the decomposition of ferric sulfate

$$Fe_2(SO_4)_3 \rightarrow Fe_2O_3 + 1.2SO_3 + 1.8SO_2 + 0.9O_2 \quad (7)$$

Table 2. Activation Energy and Pre-Exponential Factor of Ferric Sulfate Decomposition Obtained from Different Experiments and Literature

	E/R (K)	A (s^{-1})
Isothermal	28,480	1.079 E+11
Nonisothermal (10 K/min)	24,482	1.611 E+09
Kolta and Askar	26,348	1.428 E+10

The measured molar ratio of SO_2/O_2 during the experiments in the tube-reactor is about 2, further supporting the product yields proposed for this reaction.

In the grate-reactor, the injected ferric sulfate is injected into the freeboard in the form of liquid droplets with a diameter of approximately 12 mm. Upon injection, the droplets undergo water evaporation, heating, and decomposition. If we assume that each droplet generates one spherical ferric sulfate particle upon evaporation of the water, the diameter of the formed solid particle is about 6 μm, based on the density of solid ferric sulfate of 3.1 g/cm^3.[47] For such a small droplet, the water evaporation and the heating of the solid ferric sulfate particle occur on a much shorter time scale than the decomposition of ferric sulfate in the temperature range of 600–1000°C (see detailed calculations in Supporting Information). Thus, the process is assumed to be limited by ferric sulfate decomposition. In addition, because of the small size of the formed ferric sulfate particle, we assume that the decomposition of ferric sulfate is kinetically limited, that is, with negligible mass and heat transport limitations.

Gas-phase sulfation of KCl

The kinetic model proposed by Hindiyarti et al.[35] is adopted to simulate the gas-phase reactions between potassium chloride and sulfur oxides released from the decomposition of ferric sulfate. The reaction mechanism consists of subsets for hydrogen/carbon monoxide oxidation, sulfur chemistry, chlorine chemistry, potassium chemistry, and the interactions between these subsets. Hindiyarti et al.[35] validated the model by comparing predictions with results from KCl sulfation experiments carried out both at high-temperature (e.g., 1300°C) and low-temperature (e.g., 900°C) conditions. Their results indicate that the oxidation of SO_2 to SO_3 and the subsequent reactions between SO_3 and KCl constitute a mechanism for sulfation of KCl at high temperatures. At low temperatures, where formation of SO_3 from oxidation of SO_2 is negligible, sulfation of KCl is proposed to proceed through

a mechanism involving the generation and oxidation of sulfide ($KHSO_3$).[35]

Condensation of K_2SO_4

The gaseous K_2SO_4 formed from sulfation of KCl can condense both homogeneously and heterogeneously when the flue gas temperature is decreased. During biomass combustion, homogeneous condensation of K_2SO_4 primarily happens in a temperature range of 860–960°C, resulting in an aerosol with a high concentration of nanometer-sized particles.[48] The large surface area provided by these particles promotes a rapid heterogeneous condensation of K_2SO_4 and KCl, which in turn terminates the homogeneous condensation. The condensation of K_2SO_4 reduces the concentration of gaseous K_2SO_4 in the flue gas, shifting the partial equilibrium between K_2SO_4 and its precursors toward K_2SO_4, and promoting further sulfation of gaseous KCl. Following the approach of Li et al.,[37] the homogeneous and heterogeneous condensation of K_2SO_4 is approximated by a first-order reaction

$$K_2SO_4(g) \rightarrow K_2SO_4(s) \quad (8)$$

The rate constant for the process, $k_{\text{condensation}} = 1\times10^{-61}\exp(150,000/T)$,[37] represents the condensation rate predicted from aerosol theory.[48]

Model input parameters

In order to simulate the experiments carried out at the VTT grate-reactor, the postcombustion region of the reactor, that is, the region from port Y3 to Y7 in Figure 1, is modeled as an ideal plug flow reactor. The temperature profile used in the simulation (Figure 6) is based on an average of the gas temperatures measured in the different experiments. The relatively small error bars indicate that the temperature fluctuation was not significant in the experiments as they were designed to have the same combustion conditions. Thus, it is reasonable to use the measured average temperatures in the simulation. The amount and composition of the inlet flue gas are estimated based on the experiment without ferric sulfate addition, where the fuel feeding rate is 0.0075 kg/s (wet basis) and the air feeding rate is 0.05 kg/s. The flue gas is assumed to contain only N_2, O_2, CO_2, H_2O, SO_2, HCl, and KCl. The concentration of H_2O is estimated from the fuel composition, assuming that all of the H in the fuel is converted to H_2O and all of the moisture is evaporated during combustion. The flue gas concentrations of O_2, CO_2, and SO_2 are derived from the analyzed dry-based concentrations during the experiment without ferric sulfate addition. In order to obtain the inlet concentrations of KCl and HCl, mass balance calculations are performed for chorine in different experiments, according to the HCl analyzer data and the amount of Cl collected as aerosols in the impactor. The calculations show that the average fuel Cl content (0.305 wt % dry basis) estimated from the HCl and aerosol–Cl present in the flue gas is considerably larger than that of the fuel analysis (Table 1), implying that the Cl content in the fuel analysis is underestimated. Therefore, the modified fuel Cl content (0.305 wt % dry basis) is adopted to calculate the inlet concentrations of KCl and HCl used in the simulation, by assuming 100% Cl release during combustion and by using a molar ratio of HCl/KCl estimated from the relative amount of HCl and aerosol–Cl collected in the experiment without additive. The concentration of N_2 is used to balance other gas concentrations. The detailed composition of the inlet flue gas used in the modeling is given in Table 3.

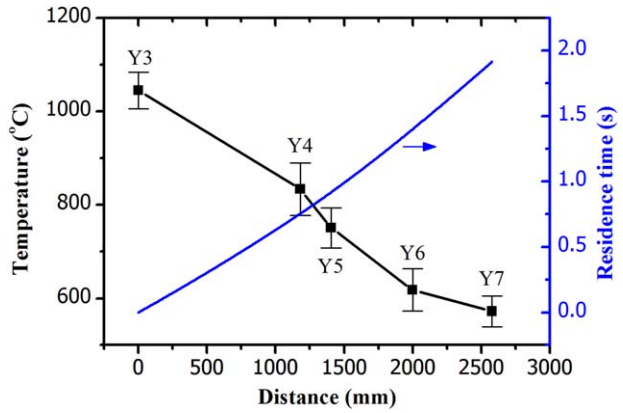

Figure 6. Temperature profile and residence time used in the simulation, from port Y3 to Y7 in Figure 1.

The solid symbols represent the average temperatures measured in different experiments, with error bar showing the standard deviation. [Color figure can be viewed in the online issue, which is available at wileyonlinelibrary.com].

Numerical approach

The simulations were carried out with CHEMKIN 4.1.1, using the plug-flow reactor model. The equation for ferric sulfate decomposition (Eq. 2) was adapted to a format compatible with CHEMKIN. The kinetic parameters were obtained from the TGA experiments under isothermal conditions (Table 2). In the model, ferric sulfate was represented as a pseudo species, SO_3* that undergoes decomposition to produce SO_2, SO_3, and O_2 according to Eq. 7. The Fe_2O_3 produced from ferric sulfate decomposition is neglected in the simulation, as we believe that it does not play an important role in gas-phase reactions. The concentration of SO_3* in the inlet flue gas was calculated from the quantity of ferric sulfate injected. For the condensation of K_2SO_4 (Eq. 8), another pseudo species, K_2SO_4(s), was introduced as the (inert) reaction product. The complete kinetic model in CHEMKIN format is available in Supporting Information. The simulation was conducted with a predefined temperature profile as shown in Figure 6. The reactor length was chosen according to the distance from Y3 to Y7 in Figure 1 (2580 mm), and the reactor diameter was 400 mm. Besides the temperature profile, a relation between the reactor length and the residence time is also shown in Figure 6.

Results and Discussion

Comparison of simulation and experimental results

Figure 7 compares the measured and simulated SO_2 concentrations at port Y7 during the experiments with different dosages of ferric sulfate. It can be seen that the emissions of SO_2 are predicted well by the model. Both the experimental

Table 3. Inlet Flue Gas Compositions Used in the Simulation

Species (unit)	Value
H_2O (%)	13.73
O_2 (%)	5.80
CO_2 (%)	12.00
SO_2 (ppmv)	28.8
HCl (ppmv)	165.2
KCl (ppmv)	65.7
N_2 (%)	balance

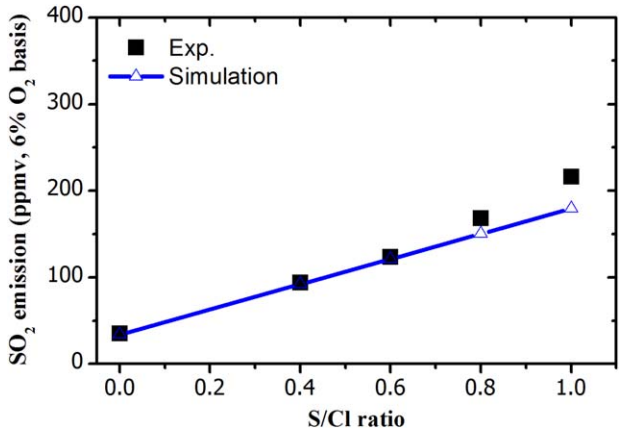

Figure 7. Simulated and measured SO_2 emissions (ppmv, 6% O_2 basis) in the dry flue gas of the VTT grate-firing experiments under different dosage of ferric sulfate ($S_{reagent}/Cl_{fuel}$ molar ratio).

The experimental SO_2 emissions are measured after the flue gas cooler (see Figure 1), whereas the simulated SO_2 emissions are obtained from port Y7. [Color figure can be viewed in the online issue, which is available at wileyonlinelibrary.com].

and the predicted results show an almost linear correlation between the dosage of ferric sulfate ($S_{reagent}/Cl_{fuel}$ molar ratio) and the emission of SO_2. The simulation results suggest that the only sulfur species at port Y7 are K_2SO_4 and SO_2 for S/Cl ratios equal to or below 0.4. When the S/Cl ratio is increased to 0.6, trace amount (around 6 ppmv, dry basis) of SO_3 appears at port Y7. However, when the S/Cl ratio is increased to 1.0, the level of SO_3 at port Y7 increases significantly to about 36 ppmv. The results indicate that an increase of S/Cl ratio from 0.6 to 1.0 may greatly promote the formation of sulfuric acid aerosols, which is qualitatively in agreement with chemical analysis of the collected submicron particles in the experiments.[31]

The predicted and measured HCl concentrations at port Y7 are compared in Figure 8. The agreement is in general

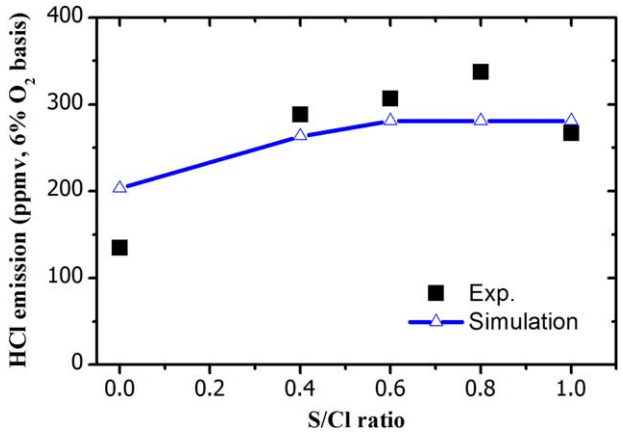

Figure 8. Simulated and measured HCl emissions (ppmv, 6% O_2 basis) in the dry flue gas of VTT grate-firing experiments with different dosages ($S_{reagent}/Cl_{fuel}$) of ferric sulfate.

Both the simulated and measured HCl emissions are from port Y7 (see Figure 1). [Color figure can be viewed in the online issue, which is available at wileyonlinelibrary.com].

satisfactory, even though HCl is overpredicted for the experiment without ferric sulfate addition (S/Cl = 0). This overprediction is mainly because the fuel Cl content (0.305 wt % dry basis) used in the simulation is an average value calculated based on all of the preformed experiments. During the experiment without ferric sulfate addition, the Cl content of the fuel was possibly smaller than the average value. Preparing a feedstock of constant composition to pilot-scale experiments from corn stover has proved to be challenging. In addition, the differences in particle shape and volumetric density of the wood chips and the crushed corn stover also lead to some difficulties in keeping a constant fuel feeding rate. Therefore, the ash content and fuel Cl concentration can fluctuate. The measured HCl emissions in Figure 8 seem to reach a plateau at S/Cl ratios in the range 0.4–1.0, indicating that the KCl in the flue gas is largely sulfated to K_2SO_4 and HCl at this level of ferric sulfate addition. This tendency is also captured well by the simulation.

In order to quantitatively describe the degree of sulfation in the experiments, the following parameter is introduced

$$\text{Degree of sulfation} = 1 - \frac{\text{Cl}}{\text{K}+\text{Na}} \tag{9}$$

where the Cl, K and Na are the relevant concentrations (mol %) in the aerosols collected at port Y5. This degree of sulfation is based on the assumption that the alkali metal found in the fine particles is comprised only of sulfates and chlorides. Thus, if all of alkalis in the aerosols are present as alkali chlorides, the calculated sulfation degree would be zero. On the other hand, if the aerosols only contain alkali sulfates, the calculated sulfation degree would be one. During the calculation of the sulfation degree in the experiments, only particles in the size range of 0.03–0.62 μm are considered in Eq. 9, because almost all of the alkali chlorides and sulfates are found in this size range and the presence of alkali silicates are negligible in these particles.[31] Therefore, it is believed that the sulfation degree calculated from the aerosols in this range is representative. In the simulation, the degree of sulfation is calculated by assuming that all of the KCl, K_2Cl_2, K_2SO_4, K_2SO_4 (s), and $KHSO_4$ found at port Y5 will end up as aerosols. This assumption is believed to be reasonable as the impactor used in the experiments for aerosol collection was operated at room temperature, meaning that all of the alkali species mentioned above would condense as aerosols during sampling and would be collected in an impactor. Thus, the relative concentrations of these species in the flue gas at port Y5 are used to calculate the sulfation degree in the simulation. Sodium is neglected in the simulation due to its small content in the fuel.

The experimental and simulated degrees of sulfation are shown in Figure 9. The degree of sulfation is close to zero in the experiment without ferric sulfate addition. When the added S/Cl ratio is 1, the experimental degree of sulfation approaches 1, indicating that almost all of the alkali chlorides are converted to alkali sulfates at port Y5 under this condition. The predicted degree of sulfation agrees well with the experimental results, although it is slightly underestimated at high S/Cl ratios. The results of Figure 9 imply that the model developed can well predict the sulfation of alkali chlorides by ferric sulfate addition under the conditions of the pilot-scale grate-firing experiments.

The experimental sulfation tendency shown in Figure 9 seems to be slightly different from that in Figure 8. According to Figure 8, an almost complete sulfation is achieved at an S/Cl ratio of 0.4–0.6, whereas in Figure 9 such a conversion degree

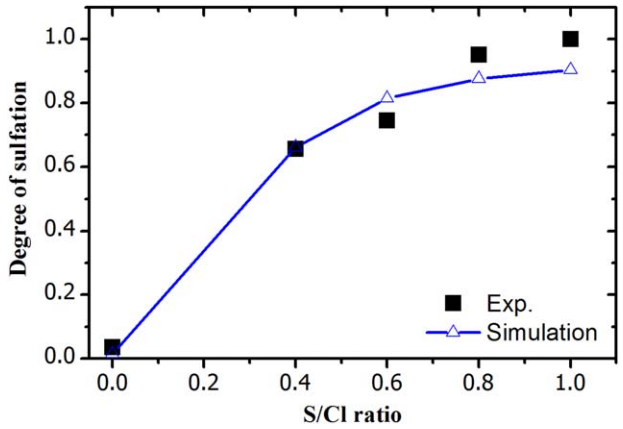

Figure 9. Simulated and measured degree of sulfation at port Y5 during the VTT grate-firing experiments with different dosage ($S_{reagent}/Cl_{fuel}$) of ferric sulfate.

[Color figure can be viewed in the online issue, which is available at wileyonlinelibrary.com].

is not reached until the S/Cl ratio becomes 1.0. A similar trend is also seen in the simulation results. As the results of Figures 8 and 9 are obtained from different sampling location (port Y5 and Y7), the discrepancy between the sulfation degree indicates that the sulfation is not completed at port Y5. Detailed analysis of the sulfation reactions under these conditions will be conducted in the following section.

Model evaluation

In order to facilitate a better understanding of the decomposition of ferric sulfate and the sulfation of KCl in the grate-firing reactor, the concentrations of the major sulfur and chlorine species along the reactor are extracted from the simulations. Figure 10 illustrates the concentration profiles obtained from the simulation with an S/Cl ratio of 0.4 and 1.0, respectively. The decomposition of ferric sulfate occurs rapidly in both cases, because of the high temperatures (~1000°C) near the injection point. After injection, the ferric sulfate is almost completely decomposed at a distance of ~270 mm, which corresponds to a residence time of ~0.16 s. The decomposition of ferric sulfate generates both SO_2 and SO_3. The SO_2 level becomes almost constant after the complete decomposition of ferric sulfate, indicating that further conversion from SO_3 to SO_2 is negligible. On the other hand, it also implies that SO_2 plays a negligible role in the sulfation of KCl under the conditions of this study.

The SO_3 produced reacts with KCl to generate both K_2SO_4 and $KHSO_4$. At temperatures above 785°C (i.e., distance < 1310 mm), only a small amount of K_2SO_4 is formed and the concentrations are similar in Figures 10a and 10b, indicating that the formation of K_2SO_4 is thermodynamically limited. The large amount of $KHSO_4$ and KCl found in this temperature range further supports that the formation of K_2SO_4 is limited by thermodynamics, as the reaction rate between $KHSO_4$ and KCl is very fast.[35] When the temperature is decreased from 785 to 720°C (in the distance of 1310–1540 mm), the gaseous K_2SO_4 is almost completely converted to solid K_2SO_4(s) through homogeneous and heterogeneous condensation as described by Eq. 8. Because of the consumption of gaseous K_2SO_4 through condensation, the formation of K_2SO_4 is no longer constrained by thermodynamics. Thus, a rapid conversion from $KHSO_4$ to K_2SO_4 is seen in the temperature range of 785–720°C.

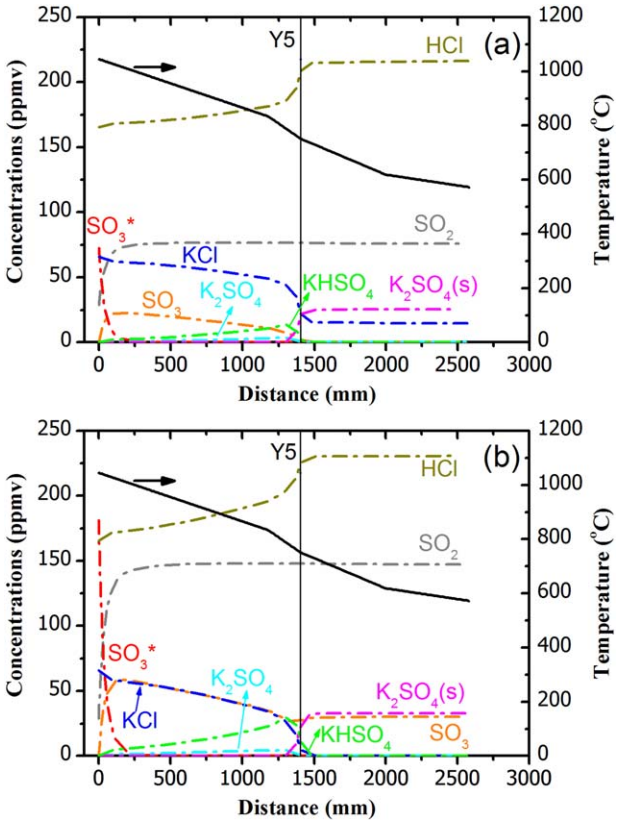

Figure 10. Temperature profile and concentration profiles of the major sulfur and chlorine species during the simulation.

(a) with a $S_{reagent}/Cl_{fuel}$ ratio of 0.4; (b) with a $S_{reagent}/Cl_{fuel}$ ratio of 1.0. The simulation covers the distance from port Y3 to Y7 in Figure 1. SO_3* represents the injected ferric sulfate; K_2SO_4(s) denotes the potassium sulfate aerosols; KCl contains both potassium chloride and its dimmer; Y5 denotes the aerosol sampling point in the experiments. [Color figure can be viewed in the online issue, which is available at wileyonlinelibrary.com].

Through a comparison of Figures 10a and 10b, it is seen that the KCl in the flue gas is only partly consumed for an S/Cl ratio of 0.4. However, when the S/Cl ratio is increased to 1.0, the KCl is almost completely converted to K_2SO_4(s). On the other hand, from both figures, it can be seen that some sulfation reactions are still going on after port Y5 (1405 mm). This explains the different sulfation degrees calculated from port Y5 and port Y7.

A pathway diagram for the potassium transformations under the conditions of Figure 10a is shown in Figure 11. The diagram is obtained from the rate-of-production (ROP) analysis in CHEMKIN, and is representative for the cases with ferric sulfation addition. According to the diagram, the sulfation of KCl under the conditions of Figure 10a is primarily achieved through the following reactions

$$KCl + SO_3(+M) = KSO_3Cl(+M) \quad (10)$$

$$KSO_3Cl + H_2O = KHSO_4 + HCl \quad (11)$$

$$KHS_4 + KCl = K_2SO_4 + HCl \quad (12)$$

The pathway diagram shown in Figure 11 differs slightly from that proposed by Hindiyarti et al.[35] According to

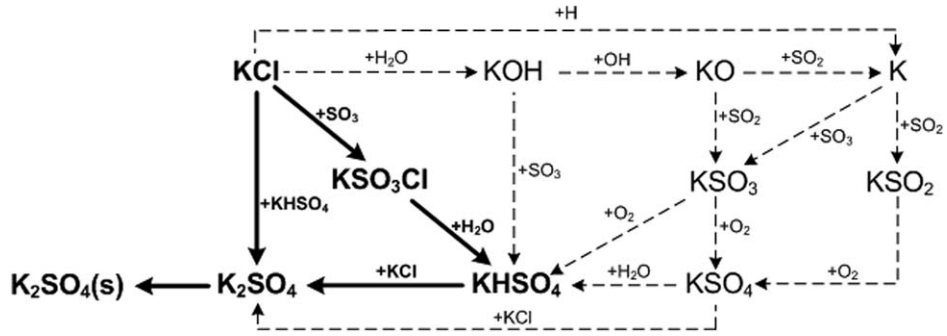

Figure 11. Pathway diagram for potassium transformations under the conditions of Figure 10a.

The dominant pathways are shown as solid lines.

Hindiyarti et al.,[35] the pathway involving the oxidation of sulfite ($KHSO_3$) to sulfate ($KHSO_4$) is important for KCl sulfation at low temperatures (e.g., 900°C). However, under the conditions of this study, the contribution of this pathway is negligible, due to the presence of a large amount of SO_3.

A first-order sensitivity analysis of the predicted K_2SO_4(s) concentration with respect to the reaction rate constants for the conditions of Figure 10a has been performed. The results corresponding to the position of port Y5 are illustrated in Figure 12. It is shown that the formation of K_2SO_4(s) is most sensitive toward the condensation of K_2SO_4 (Eq. 8). An increase of the condensation rate of K_2SO_4 would favor the formation of K_2SO_4(s). Other reactions are generally too fast to be rate limiting and their sensitivity coefficients are small.

Parametric study and practical implications

In a grate-firing combustor, gas temperature versus residence time in the furnace can vary between different pilot-scale tests. In order to evaluate the effect of temperature variation on the sulfation of KCl, simulations are carried out by shifting the temperature profile in Figure 6 by ±50°C. The results are shown in Figure 13. When the profile is shifted to lower temperatures by 50°C, the degree of sulfation at port Y5 is slightly increased. This is partly because the temperature window for the condensation of K_2SO_4 is shifted to higher positions (above port Y5) under the current condition. On the other hand, the conversion of SO_3 to SO_2 is slightly suppressed when the decomposition of ferric sulfate takes place at low temperatures, which would in turn promote the sulfation of KCl.

When the temperature profile is increased by 50°C, the degrees of sulfation at port Y5 are significantly decreased, as shown in Figure 13. This is partly because the condensation of K_2SO_4 primarily takes place after port Y5 when the temperature profile is 50°C higher. Thus, the sulfation of KCl is far from being completed at port Y5. On the other hand, even if the sulfation of KCl is completed, the obtained degree of sulfation is still lower than that obtained with the original temperature profile, as a larger fraction of SO_3 is converted to SO_2 when the decomposition of ferric sulfate happens at higher temperatures. As an example, under the condition of S/Cl = 0.6, only approximately 10% of the released SO_3 is converted to SO_2 under the original temperature profile, while this percentage is increased to about 35% when the temperature profile is increased by 50°C.

The results of Figure 13 indicate that the effectiveness of ferric sulfate addition is sensitive to temperature. It is not favorable to inject ferric sulfate at high temperatures (e.g., above 1100°C), as the produced SO_3 is converted rapidly to SO_2. On the other hand, if the ferric sulfate is injected at very low temperatures (e.g., below 800°C), the low temperature may not allow a complete decomposition of the additive, thus also affecting its effectiveness. The intermediate temperature range (e.g., between 1100°C and 800°C) is more favorable for the injection of ferric sulfate. In principle, when the detailed temperature profile in a boiler is known, the model developed in this work can be used to optimize

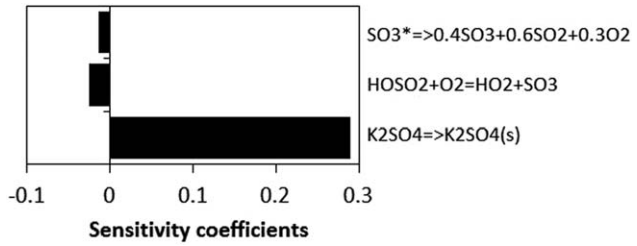

Figure 12. Sensitivity coefficients for the elementary reactions toward the K_2SO_4(s) formation under the conditions of Figure 10a, corresponding to a distance of 1405 mm (port Y5).

Only the reactions with sensitivity coefficients above 0.01 are listed.

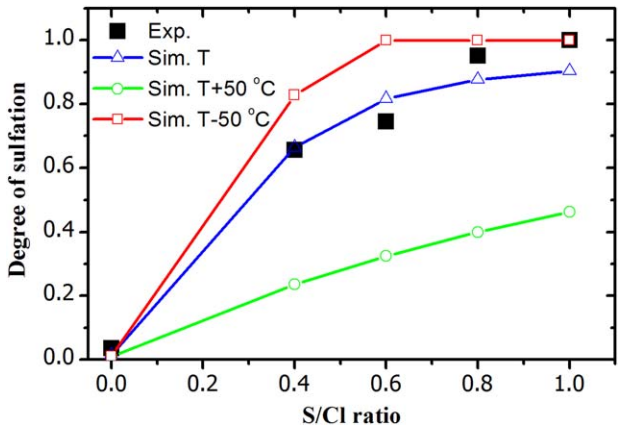

Figure 13. Simulated and measured degree of sulfation at port Y5 during the VTT grate-firing experiments with different dosage ($S_{reagent}/Cl_{fuel}$) of ferric sulfate.

The simulations are conducted by shifting the temperature profile in Figure 6 by ±50°C. [Color figure can be viewed in the online issue, which is available at wileyonlinelibrary.com].

the injection of ferric sulfate. In addition, the model can be applied to assess the level of KCl at different boiler locations during ferric sulfate injection. This knowledge may be helpful in order to evaluate the deposition and corrosion risks in the boiler.

Conclusions

Decomposition of ferric sulfate is studied in a fast-heating rate TGA and a laboratory-scale tube-reactor. The TGA experiments reveal that the decomposition of ferric sulfate can be described well by a volumetric reaction model with kinetic parameters derived from the experiments under isothermal conditions. The experiments in the laboratory scale tube-reactor imply that the sulfur released from ferric sulfate decomposition is distributed as approximately 40% SO_3 and 60% SO_2 in the temperature range of 700–1000°C.

Based on the obtained kinetic parameters and the distribution of sulfur products, a model is proposed to describe the decomposition of ferric sulfate under the conditions of a grate-firing reactor. By combining the ferric sulfate decomposition model with a detailed gas-phase kinetic model of KCl sulfation[35] and a simplified model of K_2SO_4 condensation,[37] the sulfation of KCl by ferric sulfate addition during grate-firing of biomass is simulated. The simulation results compare favorably with the experimental results obtained in a pilot-scale biomass grate-firing reactor under different dosage of ferric sulfate.[31] The simulation results suggest that the SO_3 released from ferric sulfate decomposition is the main contributor to KCl sulfation. The effectiveness of ferric sulfate addition toward KCl destruction is sensitive to the applied temperature range. For a boiler with known temperature profile and KCl level, the model developed in this work would be helpful in order to optimize the injection of ferric sulfate and to minimize deposition and corrosion risks.

Acknowledgment

Funding from EU contract 23946 "Demonstration of a 16 MW high energy efficient corn stover biomass power plant" was gratefully acknowledged.

Literature Cited

1. Jensen PA, Stenholm M, Hald P. Deposition investigation in straw-fired boilers. *Energy Fuels* 1997;11:1048–1055.
2. Yin C, Rosendahl LA, Kær SK. Grate-firing of biomass for heat and power production. *Prog Energy Combust Sci.* 2008;34:725–754.
3. Hansen LA, Nielsen HP, Frandsen FJ, Dam-Johansen K, Hørlyck S, Karlsson A. Influence of deposit formation on corrosion at a straw-fired boiler. *Fuel Process Technol.* 2000;64:189–209.
4. Michelsen HP, Frandsen F, Dam-Johansen K, Larsen OH. Deposition and high temperature corrosion in a 10 MW straw fired boiler. *Fuel Process Technol.* 1998;54:95–108.
5. Zeuthen JH, Jensen PA, Jensen JP, Livbjerg H. Aerosol formation during the combustion of straw with addition of sorbents. *Energy Fuels* 2007;21:699–709.
6. Frandsen FJ. Utilizing biomass and waste for power production—a decade of contributing to the understanding, interpretation and analysis of deposits and corrosion products. *Fuel* 2005;84:1277–1294.
7. Hupa M. Ash related issues in fluidized bed combustion of biomasses-recent research highlights. *Energy Fuels* 2012;26:4–14.
8. Åmand LE, Leckner B, Eskilsson D, Tullin C. Ash deposition on heat transfer tubes during combustion of demolition wood. *Energy Fuels* 2006;20:1001–1007.
9. Davidsson KO, Åmand LE, Steenari BM, Elled AL, Eskilsson D, Leckner B. Countermeasures against alkali-related problems during combustion of biomass in a circulating fluidized bed boiler. *Chem Eng Sci.* 2008;63:5314–5329.
10. Bashir MS, Jensen PA, Frandsen FJ, Wedel S, Dam-Johansen K, Wadenback J, Pedersen ST. Suspension-firing of biomass. Part 1: Full-scale measurements of ash deposit build-up. *Energy Fuels* 2012; 26:2317–2330.
11. Bashir MS, Jensen PA, Frandsen FJ, Wedel S, Dam-Johansen K, Wadenback J. Suspension-firing of biomass. Part 2: Boiler measurements of ash deposit shedding. *Energy Fuels* 2012;26:5241–5255.
12. Bashir MS, Jensen PA, Frandsen FJ, Wedel S, Dam-Johansen K, Wadenback J, Pedersen ST. Ash transformation and deposit build-up during biomass suspeinson and grate-firing: Full-scale experimental studies. *Fuel Process Technol.* 2012;97:93–106.
13. Frandsen FJ, van Lith SC, Korbee R, Yrjas P, Backman R, Obernberger I, Brunner T, Jöller M. Quantification of the release of inorganic elements from biofuels. *Fuel Process Technol.* 2007;88: 1118–1128.
14. van Lith SC, Alonso-Ramírez V, Jensen PA, Frandsen FJ, Glarborg P. Release to the gas phase of inorganic elements during wood combustion. Part 1: development and evaluation of quantification methods. *Energy Fuels* 2006;20:964–978.
15. van Lith SC, Jensen PA, Frandsen FJ, Glarborg P. Release to the gas phase of inorganic elements during wood combustion. Part 2: Influence of fuel composition. *Energy Fuels* 2008;22:1598–1609.
16. Knudsen JN, Jensen PA, Dam-Johansen K. Transformation and release to the gas phase of Cl, K, and S during combustion of annual biomass. *Energy Fuels* 2004;18:1385–1399.
17. Nielsen HP, Frandsen FJ, Dam-Johansen K, Baxter LL. The implications of chlorine-associated corrosion on the operation of biomass-fired boilers. *Prog Energy Combust Sci.* 2000;26:283–298.
18. Wu H, Glarborg P, Frandsen FJ, Dam-Johansen K, Jensen PA. Dust-firing of straw and additives: ash chemistry and deposition behavior. *Energy Fuels* 2011;25:2862–2873.
19. Aho M, Vainikka P, Taipale R, Yrjas P. Effective new chemicals to prevent corrosion due to chlorine in power plant superheaters. *Fuel* 2008;87:647–654.
20. Aho M, Silvennoinen J. Preventing chlorine deposition on heat transfer surfaces with aluminium – silicon rich biomass residue and additive. *Fuel* 2004;83:1299–1305.
21. Kassman H, Bäfver L, Åmand LE. The importance of SO_2 and SO_3 for sulphation of gaseous KCl – an experimental investigation in a biomass fired CFB boiler. *Combust Flame* 2010;157:1649–1657.
22. Kassman H, Broström M, Berg M, Åmand LE. Measures to reduce chlorine in deposits: application in a large-scale circulating fluidised bed boiler firing biomass. *Fuel* 2011;90:1325–1334.
23. Kassman H, Pettersson J, Steenari BM, Åmand LE. Two strategies to reduce gaseous KCl and chlorine in deposits during biomass combustion – injection of ammonium sulphate and co-combustion with peat. *Fuel Process Technol.* 2011;105:170–180.
24. Zheng Y, Jensen PA, Jensen AD. A kinetic study of gaseous potassium capture by coal minerals in a high temperature fixed-bed reactor. *Fuel* 2008;87:3304–3312.
25. Tran KQ, Iisa K, Steenari BM, Lindqvist O. A kinetic study of gaseous alkali capture by kaolin in the fixed bed reactor equipped with an alkali detector. *Fuel* 2005;84:169–175.
26. Wang L, Skjevrak G, Hustad JE, Gronli MG. Effects of sewage sludge and marble sludge addition on slag characteristics during wood waste pellets combustion. *Energy Fuels* 2011;25:5775–5785.
27. Wang L, Hustad JE, Skreiberg Ø, Skjevrak G, Grønli M. A critical review on additives to reduce ash related operation problems in biomass combustion applications. *Energy Procedia.* 2012;20:20–29.
28. Tillman DA, Duong D, Miller B. Chlorine in solid fuels fired in pulverized fuel boilers – sources, forms, reactions and consequences: a literature review. *Energy Fuels* 2009;23:3379–3391.
29. Zheng Y, Jensen PA, Jensen AD, Sander B, Junker H. Ash transformation during co-firing coal and straw. *Fuel* 2007;86:1008–1020.
30. Iisa K, Lu Y, Salmenoja K. Sulfation of potassium chloride at combustion conditions. *Energy Fuels* 1999;13:1184–1190.
31. Aho M, Paakkinen K, Taipale R. Destruction of alkali chlorides using sulphur and ferric sulphate during grate combustion of corn stover and wood chip blends. *Fuel* 2013;103:562–569.
32. Wu H, Glarborg P, Frandsen FJ, Dam-Johansen K, Jensen PA, Sander B. Trace elements in co-combustion of solid recovered fuel and coal. *Fuel Process Technol.* 2013;105:212–221.
33. Wu H, Glarborg P, Frandsen FJ, Dam-Johansen K, Jensen PA, Sander B. Co-combustion of pulverized coal and solid recovered fuel in an entrained flow reactor – general combustion and ash behaviour. *Fuel* 2011;90:1980–1991.

34. Broström M, Kassman H, Helgesson A, Berg M, Andersson C, Backman R, Nordin A. Sulfation of corrosive alkali chlorides by ammonium sulfate in a biomass fired CFB boiler. *Fuel Process Technol*. 2007;88:1171–1177.
35. Hindiyarti L, Frandsen F, Livbjerg H, Glarborg P, Marshall P. An exploratory study of alkali sulfate aerosol formation during biomass combustion. *Fuel* 2008;87:1591–1600.
36. Jørgensen TL, Livbjerg H, Glarborg P. Homogeneous and heterogeneously catalyzed oxidation of SO_2. *Chem Eng Sci*. 2007;62:4496–4499.
37. Li B, Sun Z, Li Z, Aldén M, Jakobsen JG, Hansen S, Glarborg P. Post-flame gas-phase sulfation of potassium chloride. *Combust Flame* 2013;160:959–969.
38. Wu H, Castro M, Jensen PA, Frandsen FJ, Glarborg P, Dam-Johansen K, Røkke M, Lundtorp K. Release and transformation of inorganic elements in combustion of a high-phosphorus fuel. *Energy Fuels* 2011;25:2874–2886.
39. Nielsen AR, Larsen MB, Glarborg P, Dam-Johansen K. High temperature release of SO_2 from calcined cement raw materials. *Energy Fuels* 2011;25:2917–2926.
40. Aho M, Paakkinen K, Taipale R. Quality of deposits during grate combustion of corn stover and wood chip blends. *Fuel* 2013;104:476–487.
41. Johansen JM, Aho M, Paakkinen K, Taipale R, Egsgaard H, Jakobsen JG, Frandsen FJ, Glarborg P. Release of K, Cl, and S during combustion and co-combustion with wood of high-chlorine biomass in bench and pilot scale fuel beds. *Proc Combust Inst*. 2013; 34:2363–2372..
42. Kolta G, Askar M. Thermal decomposition of some metal sulphates. *Thermochimica Acta*. 1975;11:65–72.
43. Siriwardane RV, Poston Jr JA, Fisher EP, Shen MS, Miltz AL. Decomposition of the sulfates of copper, iron (II), iron (III), nickel, and zinc: XPS, SEM, DRIFTS, XRD, and TGA study. *Appl Surf Sci*. 1999;152:219–236.
44. Wu J, Perlmutter DD. Thermal decomposition of inorganic sulfates and their hydrates. *Ind Eng Chem Process Des Dev*. 1981;20:640–646.
45. Thomas P, Hirschausen D, White R, Guerbois J, Ray A. Characterisation of the oxidation products of pyrite by thermogravimetric and evolved gas analysis. *J Therm Anal Cal*. 2003;72:769–776.
46. Yilmaz A, Hindiyarti L, Jensen AD, Glarborg P, Marshall P. Thermal dissociation of SO_3 at 1000–1400 K. *J Phys Chem A* 2006;110: 6654–6659.
47. Haynes WM, editor. CRC Handbook of Chemistry and Physics, 92nd ed. CRC Press/Taylor and Francis, Boca Raton FL, 2011.
48. Christensen KA, Livbjerg H. A plug flow model for chemical reactions and aerosol nucleation and growth in an alkali-containing flue gas. *Aerosol Sci Tech*. 2000;33:470–489.

Manuscript received Nov. 12, 2012, and revision received May. 21, 2013.